

A Bottom-Up Strategy for the Synthesis of Highly Siliceous Faujasite-Type Zeolite

Dali Zhu, Linying Wang, Dong Fan, Nana Yan, Shengjun Huang, Shutao Xu, Peng Guo, Miao Yang, Jianming Zhang, Peng Tian,* and Zhongmin Liu*

High-silica zeolite Y is a desired catalytic material for oil refining and the petrochemical industry. However, its direct synthesis remains a symbolic challenge in the field of zeolite synthesis, with a limited improvement of the framework $\text{SiO}_2/\text{Al}_2\text{O}_3$ ratio (SAR) from ≈ 5 to 9 over the past 60 years. Here, the synthesis of highly siliceous zeolite Y with tunable SAR up to 15.6 through a cooperative strategy is reported, which involves the use of FAU nuclei, a bulky organic structure-directing agent (OSDA), and a gel system with low alkalinity (named NOA-co strategy). A series of quaternary alkylammonium ions is discovered as effective OSDAs based on the NOA-co strategy, and the relevant crystallization mechanism is elucidated. Moreover, the high-silica products are demonstrated to have greatly improved (hydro)thermal stability, high concentration of strong acid sites, and uniform acid distribution, which lead to superior catalytic performance in the cracking of bulky hydrocarbons. It is anticipated that this synthetic strategy will benefit the synthesis and development of zeolitic catalysts in a wide range of reaction processes.

supercages (≈ 1.12 nm diameter). The introduction of zeolite Y has revolutionized the fluid catalytic cracking (FCC) and hydrocracking processes in oil refinery owing to its large pore openings and strong acidity.^[3] In recent years, FAU-type zeolites also show interesting potential as efficient catalysts to convert biomass into fuels and chemicals.^[4] However, zeolite Y has been well known with its physique of Al-rich framework, which brings a fatal drawback in hydrothermal stability toward its practical applications.^[5] To alleviate this issue, repeated dealumination processes have been employed in order to achieve the high-silica counterparts.^[6] These post-treatment procedures are complicated and time/energy-consuming.^[7] In addition, dealumination gradient is inevitable, which brings unfavorable outcomes for their catalytic applications.^[8]


Zeolites, crystalline aluminosilicates with well-defined micro- porosities, play a fundamental role in the production of energy and chemicals.^[1] The applications of zeolites have brought breakthrough innovations in the fields of heterogeneous catalysis and adsorption separation.^[2] Among them, zeolite Y is one of the most important zeolites, which belongs to the FAU family with 3D 12-membered ring (MR) channels and spherical

Although considerable progress has been achieved in composition and morphology control of zeolites over the past decades, it remains a symbolic challenge for the synthesis of high-silica zeolite Y. The value of 6–7 is the maximum framework SAR for zeolite Y synthesized from inorganic hydrogel.^[9] The obstacle to improve the framework SAR of zeolite Y lies in the mismatch between the alkalinity requirement of nucleation/crystallization rate and high framework SAR.^[10] High alkalinity gel system facilitates the nucleation and crystallization processes, but generally results in low framework SAR due to the increased solubility of silica in it. Lowering the gel alkalinity can help the formation of more siliceous polymeric intermediates and products, which, however, would cause incomplete crystallization because of increased energy barrier for nucleation and crystal growth.^[11] The introduction of organic structure-directing agent (OSDA) with low charge density theoretically offers an effective way to improve the SAR,^[12] and the crystallization kinetics may also be accelerated by virtue of enhanced host-guest interactions in the presence of OSDAs.^[13] Unfortunately, only few OSDAs have been discovered for FAU-type zeolite syntheses after extensive exploration for decades. The highest SAR ever reported for the direct synthesis of zeolite Y was limited to 9 by employing 15-crown-5 ether as an OSDA.^[14] Thus, to find effective synthesis strategy for high-silica zeolite Y is greatly desirable from the viewpoint of both fundamental research and industrial applications.

D. Zhu, Dr. L. Wang, Dr. D. Fan, N. Yan, Prof. S. Xu, Dr. P. Guo, Prof. M. Yang, J. Zhang, Prof. P. Tian, Prof. Z. Liu
National Engineering Laboratory for Methanol to Olefins
Dalian National Laboratory for Clean Energy
Dalian Institute of Chemical Physics
Chinese Academy of Sciences
Dalian 116023, P. R. China
E-mail: tianpeng@dicp.ac.cn; liuzm@dicp.ac.cn

D. Zhu, N. Yan
University of Chinese Academy of Sciences
Beijing 100049, P. R. China

Prof. S. Huang
Division of Fossil Energy Conversion
Dalian National Laboratory for Clean Energy
Dalian Institute of Chemical Physics
Chinese Academy of Sciences
Dalian 116023, P. R. China

 The ORCID identification number(s) for the author(s) of this article can be found under <https://doi.org/10.1002/adma.202000272>.

DOI: 10.1002/adma.202000272

NOA-co strategy

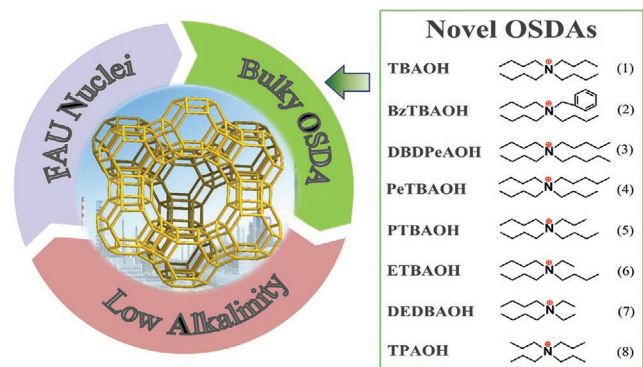


Figure 1. The NOA-co strategy and novel OSDAs for the synthesis of high-silica zeolite Y.

Herein, we report the facile synthesis of the most siliceous zeolite Y (named SY zeolite) with tunable SAR up to 15.6 by a novel cooperative strategy (Figure 1), in which FAU nuclei, bulky OSDA and gel system with low alkalinity work together and contribute to the crystallization of high-silica FAU framework (named NOA-co strategy). The FAU nuclei, which provide highly active nanocrystallites for the synthesis, could help to overcome the difficulty in zeolite nucleation. The bulky OSDA together with the assistance of Na^+ is in charge of the crystal growth of high-silica FAU structure under lower alkalinity. As the low charge density of bulky OSDA and the weak alkalinity of gel system are not conducive to zeolite nucleation,^[15] the presence of FAU nuclei in the NOA-co strategy is therefore necessary, which can reduce the requirement for nucleation ability of bulky OSDA and widen the selection scope of OSDAs. Notably, eight bulky OSDAs (quaternary alkylammonium ions) have been discovered by using the NOA-co strategy (Figure 1). Among them, tetrabutylammonium hydroxide (TBAOH) is the most powerful one with broad phase region for the formation of high-silica zeolite Y.

The synthesis conditions and product compositions of SY zeolites based on TBAOH system are presented in Table 1. The effect of reagent sources on the synthesis is displayed in

Table S1, Supporting Information. The synthetic procedures include the preparation of FAU nuclei solution and its subsequent addition to the low-alkalinity gel with TBAOH. The molar composition of the starting nuclei solution can be expressed as $1 \text{ SiO}_2: 0.1 \text{ Al}_2\text{O}_3: 0.01 \text{ Na}_2\text{O}: 0.6 (\text{TEA})_2\text{O}: 18.3 \text{ H}_2\text{O}$ (hydrothermal aging condition: 50°C for 12 h and then 100°C for 48 h). The advantages of the use of nuclei solution herein are twofold: 1) there is no need for product separation; and 2) it ensures the high dispersion (high activity) of FAU nanocrystallites. As illustrated in Table 1, the crystallization could be successfully completed under much wider gel SAR at 120°C , and the total $(\text{OH})^-/\text{SiO}_2$ ratios (including the contribution of organic bases) are lower than those of inorganic hydrogel systems,^[9b,16] demonstrating the effectiveness of the NOA-co strategy. The product SAR shows a clear rising trend as the decreasing gel alkalinity or the increasing gel SAR. However, excessively low alkalinity would cause the formation of Beta impurity and higher gel SAR (≥ 70) leads to ZSM-5. The SY zeolite with the highest SAR of 15.6 (sample SY_{15.6}) is synthesized from an initial gel with molar composition of $1 \text{ SiO}_2: 1/x \text{ Al}_2\text{O}_3: \gamma \text{ Na}_2\text{O}: 0.10 (\text{TBA})_2\text{O}: 20 \text{ H}_2\text{O}$ ($x = 60, \gamma = 0.10$) together with the addition of FAU nuclei solution (Table 1). Such a SAR value represents the highest record ever reported for the directly synthesized zeolite Y.

The XRD patterns of the SY samples are shown in Figure 2 and Figure S1, Supporting Information, which exhibit the characteristic diffraction peaks of FAU structure. An obvious shift of the peaks to high angle can be observed when comparing the XRD pattern of SY_{15.6} with NaY_{ref} (insert in Figure 2a), which consists with the decreased unit cell of the high-silica framework. The SEM images (Figure S1, Supporting Information and Figure 2) reveal that the SY samples have the octahedral morphology in sizes of 100–250 nm. The textural properties of the samples are given in Table S2, Supporting Information. In comparison with commercial NaY_{ref} , the SY samples possess larger micropore surface areas, confirming their high crystallinity. Moreover, they also exhibit higher external surface areas, which are in accordance with their small crystal sizes and would benefit the catalytic applications due to the enhancement of mass transfer.^[17]

Table 1. Syntheses and product properties of the high-silica SY zeolites.

Sample	Time [day]	$x^a)$	$\gamma^a)$	$\text{SiO}_2/\text{Al}_2\text{O}_3^b)$	$(\text{OH})^-/\text{SiO}_2^b)$	Product			
						Phase	$\text{SiO}_2/\text{Al}_2\text{O}_3^c)$	$\text{Na}_2\text{O}/\text{Al}_2\text{O}_3^c)$	$(\text{TBA}^+/\text{TEA}^+)^d)$
SY _{10.2}	3.5	20	0.12	18.3	0.51	FAU	10.2 (10.0)	0.58	
SY _{11.2}	4.5	20	0.10	18.3	0.47	FAU	11.2 (11.3)	0.56	1.3
SY _{11.6}	5.5	20	0.09	18.3	0.45	FAU	11.6	0.54	
SY _{BEA}	6.0	20	0.08	18.3	0.44	FAU (BEA)			
SY _{12.7}	3.5	30	0.10	25.4	0.47	FAU	12.7 (12.9)	0.52	2.6
SY _{14.1}	4.5	40	0.10	31.4	0.47	FAU	14.1 (14.3)	0.47	3.6
SY _{15.6}	6.5	60	0.10	41.3	0.47	FAU	15.6 (15.7)	0.50	4.0
SY _{MFI}	7.0	70	0.10	45.3	0.47	FAU (MFI)			

^{a)}Initial gel: $1\text{SiO}_2: 1/x\text{Al}_2\text{O}_3: \gamma\text{Na}_2\text{O}: 0.10(\text{TBA})_2\text{O}: 20\text{H}_2\text{O}$; FAU nuclei solution: $1\text{SiO}_2: 0.10\text{Al}_2\text{O}_3: 0.01\text{Na}_2\text{O}: 0.6(\text{TEA})_2\text{O}: 18.3\text{H}_2\text{O}$ (hydrothermal aging condition: 50°C for 12 h and then 100°C for 48 h). The addition of nuclei solution into the initial gel is 10 wt% (based on SiO_2). The crystallization temperature for the final gel is 120°C ;

^{b)} $\text{SiO}_2/\text{Al}_2\text{O}_3$ and $(\text{OH})^-/\text{SiO}_2$ molar ratios in the final gel, which contain the contribution of the sources from the nuclei solution; ^{c)}Measured by XRF. The value in the bracket is calculated based on ^{29}Si MAS NMR; ^{d)}Deduced from CHN elemental analysis.

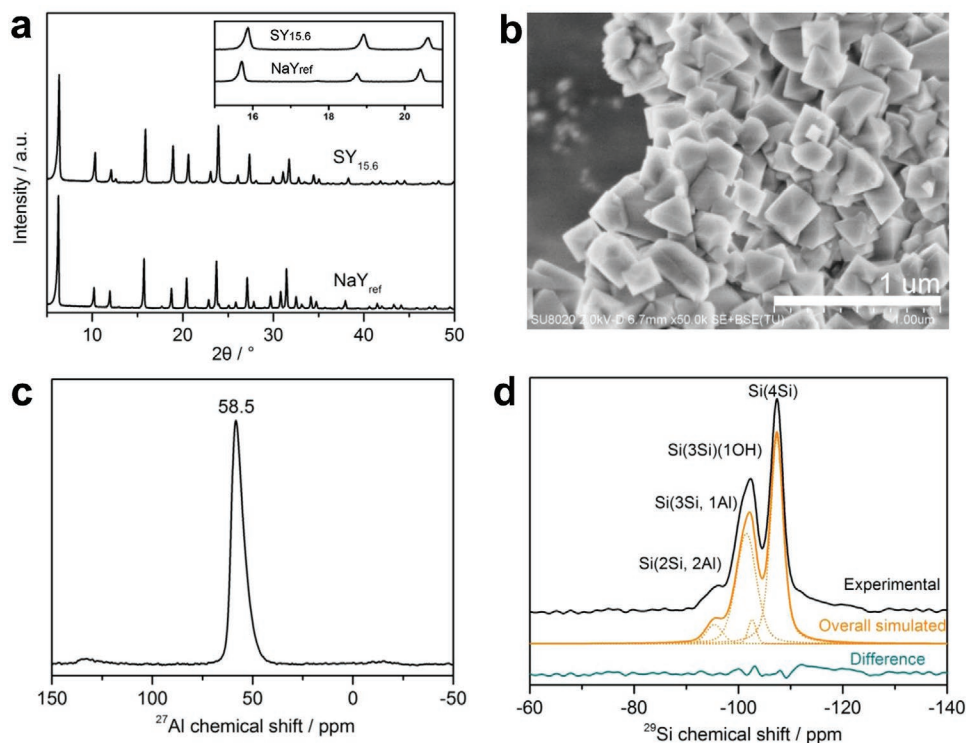


Figure 2. a) XRD patterns of the as-made $\text{SY}_{15.6}$ and commercial NaY_{ref} (SAR = 5.6), b) SEM image, and c) ^{27}Al and d) ^{29}Si MAS NMR spectra of the as-made $\text{SY}_{15.6}$.

The ^{27}Al and ^{29}Si MAS NMR spectra of the as-made $\text{SY}_{15.6}$ are illustrated in Figure 2. The ^{27}Al spectrum evidences the sole existence of tetrahedral-coordinated Al species in the framework. Two strong resonances ascribed to Si(4Si) and Si(3Si, 1Al) species dominate in the ^{29}Si spectrum. Moreover, the slight asymmetry for the peak at -101 ppm suggests the existence of small amount of silanol species.^[18] This assignment is confirmed by $^1\text{H}/^{29}\text{Si}$ CP MAS NMR spectra showing an obvious increase of the signal at -102 ppm and by FT-IR spectrum with the appearance of the peak at 3738 cm^{-1} attributed to isolated external silanols (Figure S2, Supporting Information).^[19] According to the deconvoluted ^{29}Si spectrum (Table S3, Supporting Information), the framework SAR of $\text{SY}_{15.6}$ is calculated to be 15.7, which is in good agreement with the value derived from XRF. The weak broad peak at around -112 ppm in the difference spectrum of (d) suggests that there may exist tiny amount of amorphous silica. The ^{13}C MAS NMR spectrum shown in Figure S2, Supporting Information demonstrates the coexistence of TBA^+ and TEA^+ in the as-made samples (TEA^+ is from the nuclei solution). The molar ratio of TBA^+ to TEA^+ was estimated to be 4.0 for $\text{SY}_{15.6}$ based on the CHN elemental analysis. Moreover, a rising trend of $\text{TBA}^+/\text{TEA}^+$ ratios for SY samples can be found from 1.3 to 4.0 with the increased framework SAR from 10.2 to 15.7 (Table 1), implying that TBA^+ is the predominant OSDA in forming the high-silica framework. According to the combined analyses of XRF, CHN elemental analysis and TG results, the unit cell compositions of SY samples are determined and shown in Table S4, Supporting Information. We further tried to use Rietveld refinement to identify the locations of guest species occluded in the SOD cages and

supercages of the as-made SY sample (Figure S3, Supporting Information). It reveals that each SOD cage is occupied by one Na^+ ion. But the high symmetry of FAU framework and the diversity and flexibility of OSDAs result in complicated electron density clouds within the supercages, which disable the interpretation of the locations of OSDAs.

To understand the formation and growth of SY zeolites, the FAU nuclei solution and the subsequent crystallization process were examined. As displayed in Figure 3, the initial solution was highly transparent, which evolved to a colloid suspension after hydrothermal aging. The XRD pattern (Figure 3c) of the solid extracted from the nuclei solution is much broad and weak, which presents the characteristic peaks of FAU-type zeolite, implying the formation of nanosized Y crystals. HRTEM investigation (Figure 3d,e) reveals that the nanoparticles have clear lattice fringes and in sizes of 10–40 nm. The particle size distribution of the collected solid by DLS analysis (Figure 3b) is consistent with the HRTEM result, which, however, is clearly larger than that of the nuclei solution. Given the low yield of the collected solid, we speculate that more ultra-small nanocrystallites may exist in the nuclei solution. This is well supported by the smooth crystallization of SY zeolite using the “solid-free” nuclei solution (prepared via high-speed centrifugation).

The crucial role of the FAU nuclei in the synthesis can be demonstrated by designed control experiments (Figure S4, Supporting Information): 1) with the addition of initial clear solution; 2) with the addition of solid NaY_{ref} crystals (only TBAOH as OSDA); 3) with the addition of nanocrystallites collected from FAU nuclei solution (only TBAOH as OSDA). Only amorphous product is obtained in (1), and very weak

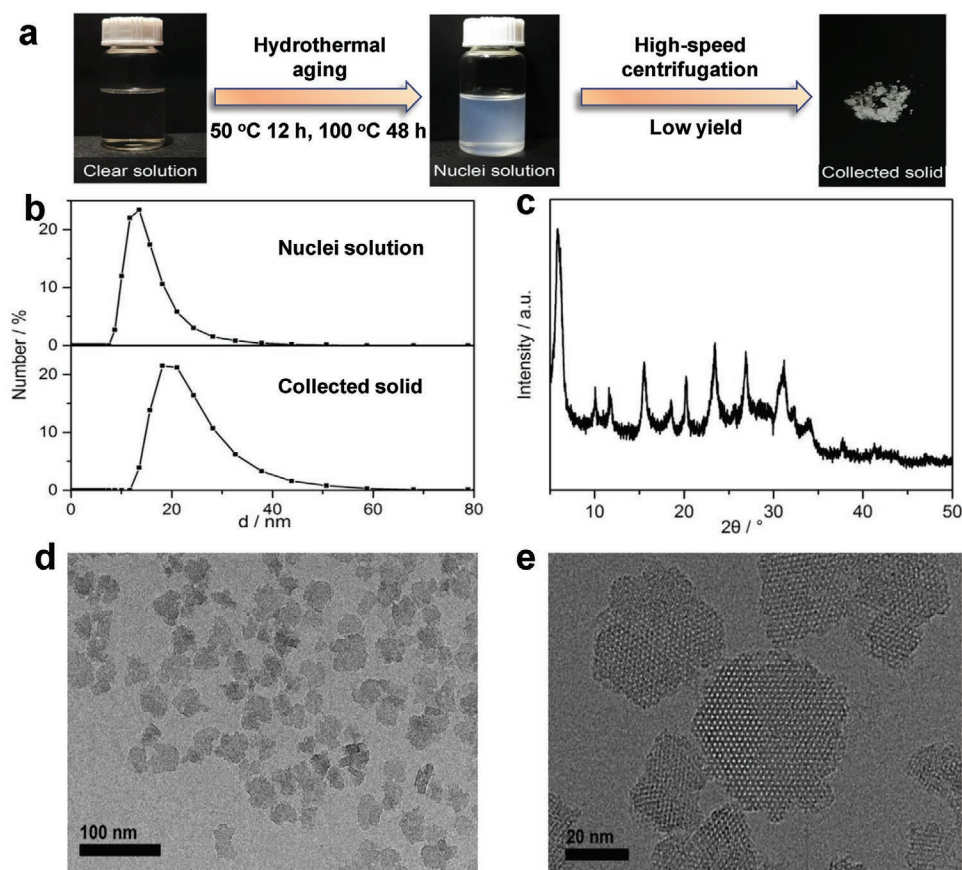


Figure 3. a) Photographs of the nuclei solution before and after hydrothermal aging, b) DLS analyses of the nuclei solution and the solid extracted from nuclei solution by high-speed centrifugation of 20000 rpm, c) XRD pattern, and d,e) HRTEM images of the collected solid.

XRD peaks are observed for the product of 2). However, well-crystallized high-silica zeolite Y is achieved in 3), which evidences the vital effect of the nanocrystallites in the nuclei solution and also confirms TBAOH rather than TEOH indispensable for the synthesis of SY zeolites. These results demonstrate that the introduction of highly active FAU nuclei can effectively help circumvent the difficulty in nucleation, and provide more opportunities for the bulky TBAOH to play its role in directing the crystal growth.

The crystallization process was investigated based on the synthetic system of sample SY_{14.1}. An induction period of about 2 days can be observed before the fast growth of high-silica zeolite Y (Figure S5a, Supporting Information). HRTEM images (Figure S5d, Supporting Information) reveal the existence of nanocrystals in the solids extracted at the induction period of crystallization. An interplanar spacing of 1.418 nm can be identified for the nanocrystals, which corresponds to the (111) lattice planes of the FAU framework and evidences the good stability of these nanocrystals. The amount of nanocrystallites increases as the crystallization proceeds, as revealed by HRTEM images and the incremental micropore area (Figure S5b, Supporting Information). After 3 days of heating, the characteristic octahedral morphology of zeolite Y becomes apparent, and their sizes grow larger along with the gradual diminishing of amorphous materials (Figure S6, Supporting Information). The crystallization is complete after about 4.5 days.

Table S5, Supporting Information summarizes the solid yields and elemental compositions of the solid/liquid phases collected at different crystallization times. Both the solid yield and solid SAR show an obvious decrease at the initial stage (0.5 day) and then maintain at almost constant values until the end of the crystallization. N₂ physisorption reveals the early solid products (Figure S5c, Supporting Information) have obviously enlarged pore sizes compared to the SiO₂ source. Meanwhile, SEM-EDX analyses (Figure S7, Supporting Information) demonstrate the homogeneous elemental distribution of Si/Al/Na in the solid particles of 0.5 day. It is thus speculated that fast reactions between mesoporous silica gel and Al source occur upon heating, and the SiO₂ domains without the protection of Al dissolve into the solution.^[10] TEA⁺ cations are detected in all solid samples. The contents of Na⁺ and TEA⁺ in the solids show little variation in the first 2.5 days. Afterward, their contents drop gradually together with the appearance of TBA⁺. The content of TBA⁺ in the solids increases until the end of the crystallization, in parallel to the formation of crystallized products. Thus, the crystallization process of SY zeolites is speculated as follows (Figure 4): i) the rapid formation of meso/macroporous TEA⁺/Na⁺/aluminosilicate composites upon mixing/heating and the dissolution of SiO₂ source having no/less interactions with Al species; ii) the growth/accumulation of FAU nuclei and the local solid–solid rearrangement on the surface of TEA⁺/Na⁺/aluminosilicate particles (the latter involves the participation

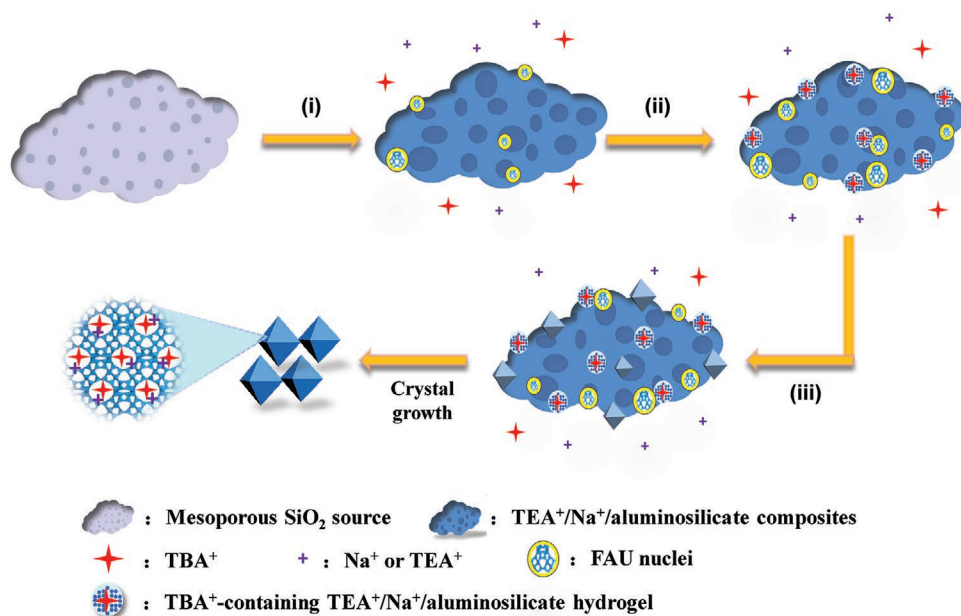


Figure 4. Proposed formation mechanism of high-silica SY zeolite by the NOA-co strategy.

of TBA⁺ from the liquid phase); iii) the migration and attachment of these organized TBA⁺-containing hydrogels to the FAU nuclei, on which surface-induced nucleation works and contributes to the crystal growth.^[20] This proposed mechanism is also supported by designed dry gel conversion (DGC) experiment, in which dry gel prepared from the 12 h hydrothermal gel (via filtration and dry) can be transferred to well-crystallized high-silica zeolite Y with similar SAR to its hydrothermal counterpart (the mother liquid separated was used as liquid phase for the DGC experiment).

Based on the NOA-co strategy, we also succeed in further improving the SAR of zeolite Y with the known OSDAs such as TEOH and 15-crown-5 (samples SY-TEAOH_{8,9} and SY-15-crown-5_{10,2} in Figure S8 and Table S2, Supporting Information).^[14,21] This should be owing to the allowed lower gel alkalinity in the presence of highly active FAU nuclei. Given the structural similarity of TEOH and TBAOH, it is speculated that other quaternary alkylammonium ions with similar structures may also be effective for the synthesis. We thus selected eight bulky OSDAs for the synthesis exploration. Fortunately, seven of them (Figure 1, 2–8) can readily deliver well-crystallized products with SAR of 8.6–13.1 (Figure S9, Supporting Information). However, when using more bulky tetrapentylammonium hydroxide (TPeAOH) as an OSDA, the crystallization cannot be initiated even after 5 days. According to these results, we believe that more quaternary alkylammonium ions with structures as illustrated in Figure S10, Supporting Information have the possibility for the synthesis of high-silica zeolite Y by NOA-co strategy. Moreover, the above results suggest that the effectiveness of bulky OSDAs for the synthesis of SY should be closely related to their structures and charge densities. The OSDAs with relatively high charge densities (such as TPAOH and DEDBAOH, Figure S9, Supporting Information) lead to products with lower SAR due to their smaller size and thus higher OSDA number occluded in the FAU supercage (more

Al atoms have to be incorporated into the framework to balance the OSDA cations). The highest SAR achieved on TBAOH is possibly a balance result between the charge density and crystallization kinetics.

Additionally, the synthetic strategy is demonstrated to be effective for the improvement of SAR of other zeolites. For example, nanosized high-silica EMT zeolite (SAR = 11.4, named NOA-EMT_{11,4}) has been synthesized by using its known OSDA 18-crown-6 ether (Figure S11 and Table S2, Supporting Information). The SAR of NOA-EMT_{11,4} is higher than the best record (SAR = 9.8) and the crystallization time is dramatically shortened from 40 to 5.5 days.^[14] Given that EMT zeolite is a hexagonal polytype of the cubic FAU zeolite and has 3D 12-MR channels, NOA-EMT_{11,4} with nanosheets morphology, large external surface area (172 m² g⁻¹) and mesopore volume (0.27 cm³ g⁻¹) is expected to be interesting catalyst for the conversion of hydrocarbons.

The thermal and hydrothermal stabilities of zeolites are important for their industrial applications.^[5b,22] The thermal analysis curves displayed in Figure S12, Supporting Information reveal that the structural collapse temperatures of the samples have an order of SY_{15,6} > SY_{10,2} > NaY_{ref}. The hydrothermal stability investigation was conducted based on the H-form samples. The textural properties of the samples before and after steam treatment are characterized and presented in Figure S12, Supporting Information. For H-SY samples, about 80% of their micropore volume was retained after 100% steam treatment at 750 °C for 2 h, much higher than that of H-Y_{ref} (30%) treated under the same conditions. In particular, even after steam treatment at 800 °C for 18 h, H-SY_{10,2}, and H-SY_{15,6} can still preserve more than 60% of their micropore volume. These results highlight the excellent thermal and hydrothermal stabilities of SY zeolites, which are owing to their increased framework SAR.

1,3,5-Triisopropylbenzene (TIPB) and n-dodecane were used as model feedstocks to probe the catalytic cracking

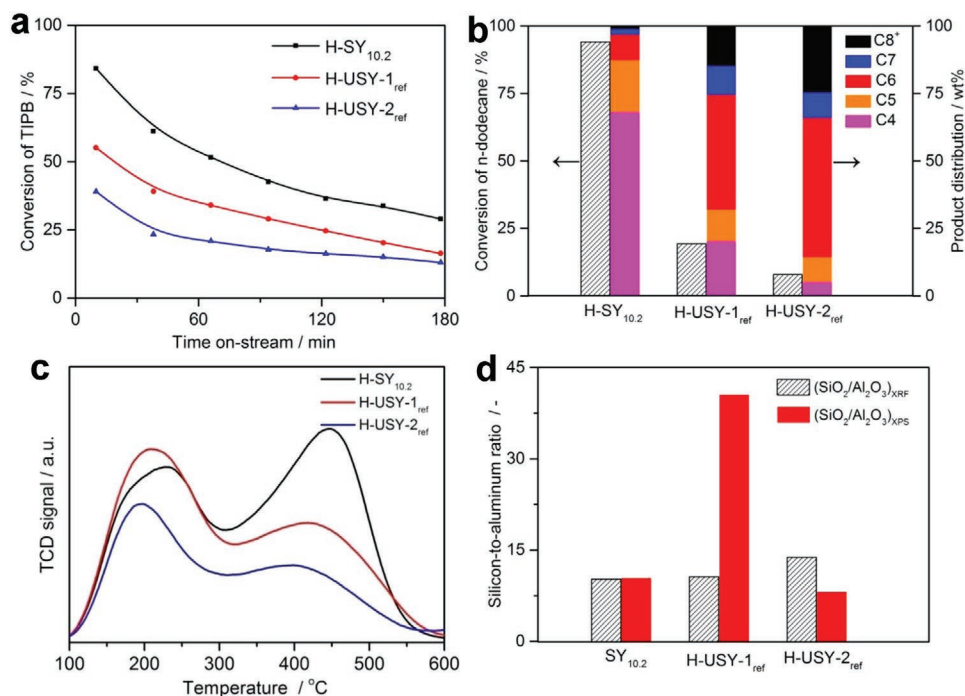


Figure 5. The catalytic cracking of hydrocarbons, acidity and product SAR on H-SY_{10.2} compared to commercial H-USY-1_{ref} and H-USY-2_{ref}. a) 1,3,5-triisopropylbenzene (TIPB) cracking versus time on stream. Reaction conditions: $T = 160\text{ }^{\circ}\text{C}$, $\text{WHSV}_{\text{TIPB}} = 4.1\text{ h}^{-1}$; b) N-dodecane conversion and products distribution. Reaction conditions: $T = 250\text{ }^{\circ}\text{C}$, $\text{WHSV}_{\text{n-dodecane}} = 50.0\text{ h}^{-1}$, TOS = 2 min; c) NH_3 -TPD; d) bulk and surface SAR of the samples determined by XRF and XPS, respectively.

performance of H-form SY zeolites (Figure 5). Herein, SY_{10.2} was selected as catalyst for the reaction (Figure S13, Supporting Information), and two high-quality ultrastable USY_{ref} with comparable SAR to SY_{10.2} as reference catalysts (Figure S14 and Table S2, Supporting Information). USY-1_{ref} and USY-2_{ref} were prepared by typical dealumination methods from conventional zeolite Y by ammonium hexafluorosilicate (AHFS) and steam treatment, respectively. In the case of TIPB cracking, H-SY_{10.2} exhibits higher conversion and cracking depth (Table S6, Supporting Information) than reference samples. As the kinetic diameter of TIPB molecule (0.95 nm) is larger than the pore opening of zeolite Y, the cracking of TIPB should occur on the external surface of the catalysts, suggesting a large number of acid sites located at the external surface of H-SY_{10.2}. The n-dodecane conversion and the corresponding products distribution are displayed in Figure 5b. Under identical reaction conditions, the n-dodecane conversion on H-SY_{10.2} is 94.1%, which is 4.9-fold and 11.9-fold higher than those over H-USY-1_{ref} and H-USY-2_{ref} respectively. Moreover, H-SY_{10.2} also displays higher cracking degree, which is consistent with the superior conversion on it.

The distinct catalytic performance of the catalysts suggests their difference in acid sites density and acid distribution. The NH_3 -TPD results (Figure 5c) demonstrate that H-SY_{10.2} possesses more strong acid sites than commercial H-USY samples. Besides, distinct Al distributions among the three samples have been revealed by XPS (Figure 5d). The surface SAR of SY_{10.2} is close to its bulk SAR, implying a homogeneous acid sites distribution in the crystals. Nevertheless, USY-1_{ref} gives a much higher SAR_{surface} (40.5) than its SAR_{bulk} (10.6). This is

reasonable considering that dealumination by AHFS is a diffusion-controlled process, which would cause Al gradient in the crystals and Si deposition on the outer shell of the crystals.^[23] For USY-2_{ref}, lower SAR_{surface} (8.1) is found and there is a significant amount of extra framework Al species (EFAL) (Figure S14c, Supporting Information). Such features should result from the migration of EFAL species to the crystal surface during steam treatment.^[24] The surface Si or Al deposition observed for commercial USY samples not only reduces the concentration of acid sites on the external layer, but causes a decrease in the accessibility of internal acid sites. Therefore, the higher concentration of external acid sites and larger external surface area of H-SY_{10.2} provide more opportunity for the TIPB molecules to be cracked. Regarding the cracking of n-dodecane, the superior catalytic activity of H-SY_{10.2} should result from its abundant strong acid sites, uniform acid distribution, and small crystal size. These results clearly demonstrate the advantages of high-silica SY zeolite in catalytic cracking, which is expected to be more prominent when processing increasingly heavy feedstocks.^[3d]

In summary, the NOA-co strategy developed in this work opens up the way for the direct synthesis of high-silica zeolite Y. Eight bulky quaternary alkylammonium ions have been discovered as effective OSDAs, among which TBAOH is the most powerful one with wide synthesis phase region and the highest SAR of 15.6. The structural features of OSDAs which have the possibility for the synthesis of SY zeolites have also been proposed. The high SAR of SY zeolites endows them with excellent (hydro)thermal stability and superior catalytic cracking activities. Given that this strategy has been proven to be effective

for the SAR improvement of EMT zeolite, it is expected that it can be extended to other types of low silica zeolites. Moreover, the high-silica SY zeolites offer exciting opportunities for fundamental study and industrial applications in adsorption, separations and catalysis involving bulky molecules, especially for the FCC and hydrocracking processes.

Supporting Information

Supporting Information is available from the Wiley Online Library or from the author.

Acknowledgements

D.Z. and L.W. contributed equally to this work. This work was supported by the National Natural Science Foundation of China (21676262, 21991091), the Key Research Program of Frontier Sciences, CAS (QYZDB-SSW-JSC040, QYZDY-SSW-JSC024), and DICI Funding (DICI ZZBS201807). The authors thank Prof. Peng Xie for helpful discussion about the catalysis.

Conflict of Interest

The authors declare no conflict of interest.

Keywords

catalytic cracking, Faujasite-type zeolites, organic structure-directing agents, zeolite synthesis, zeolite Y

Received: January 13, 2020
Revised: April 27, 2020
Published online: May 20, 2020

- [1] J. Shi, Y. Wang, W. Yang, Y. Tang, Z. Xie, *Chem. Soc. Rev.* **2015**, *44*, 8877.
- [2] C. Martínez, A. Corma, *Coord. Chem. Rev.* **2011**, *255*, 1558.
- [3] a) W. Vermeiren, J.-P. Gilson, *Top. Catal.* **2009**, *52*, 1131; b) K. P. de Jong, J. Zecevic, H. Friedrich, P. E. de Jongh, M. Bulut, S. van Donk, R. Kenmogne, A. Finiels, V. Hulea, F. Fajula, *Angew. Chem. Int. Ed.* **2010**, *49*, 10074; c) E. T. C. Vogt, B. M. Weckhuysen, *Chem. Soc. Rev.* **2015**, *44*, 7342; d) J. Garcia-Martinez, K. Li, G. Krishnaiah, *Chem. Commun.* **2012**, *48*, 11841; e) A. Corma, *Chem. Rev.* **1995**, *95*, 559.
- [4] a) L. Tao, Z. J. Wang, T. H. Yan, Y. M. Liu, H. Y. He, Y. Cao, *ACS Catal.* **2017**, *7*, 959; b) R. M. West, M. S. Holm, S. Saravanamurugan, J. M. Xiong, Z. Beversdorf, E. Taarning, C. H. Christensen, *J. Catal.* **2010**, *269*, 122.
- [5] a) G. Agostini, C. Lamberti, L. Palin, M. Milanese, N. Danilina, B. Xu, M. Janusch, J. A. van Bokhoven, *J. Am. Chem. Soc.* **2010**, *132*, 667; b) B. Xu, S. Bordiga, R. Prins, J. A. van Bokhoven, *Appl. Catal., A* **2007**, *333*, 245.
- [6] a) D. Verboekend, G. Vile, J. Perez-Ramirez, *Adv. Funct. Mater.* **2012**, *22*, 916; b) M. C. Silaghi, C. Chizallet, P. Raybaud, *Microporous Mesoporous Mater.* **2014**, *191*, 82.
- [7] a) Y. Fan, H. Xiao, G. Shi, H. Liu, Y. Qian, T. Wang, G. Gong, X. Bao, *J. Catal.* **2011**, *279*, 27; b) L. Kubelkova, S. Beran, A. Malecka, V. M. Mastikhin, *Zeolites* **1989**, *9*, 12.
- [8] a) Z. X. Qin, K. A. Cychosz, G. Melinte, H. El Siblani, J. P. Gilson, M. Thornmes, C. Fernandez, S. Mintova, O. Ersen, V. Valtchev, *J. Am. Chem. Soc.* **2017**, *139*, 17273; b) Q. L. Wang, M. Torrealba, G. Giannetto, M. Guisnet, G. Perot, M. Cahoreau, J. Caisso, *Zeolites* **1990**, *10*, 703; c) Z. Qin, B. Shen, X. Gao, F. Lin, B. Wang, C. Xu, *J. Catal.* **2011**, *278*, 266.
- [9] a) M. D. Oleksiak, K. Muraoka, M. F. Hsieh, M. T. Conato, A. Shimojima, T. Okubo, W. Chaikittisilp, J. D. Rimer, *Angew. Chem., Int. Ed.* **2017**, *56*, 13366; b) H. Awala, J. P. Gilson, R. Retoux, P. Boullay, J. M. Goupil, V. Valtchev, S. Mintova, *Nat. Mater.* **2015**, *14*, 447.
- [10] R. Li, N. Linares, J. G. Sutjianto, A. Chawla, J. Garcia-Martinez, J. D. Rimer, *Angew. Chem., Int. Ed.* **2018**, *57*, 11283.
- [11] a) S. Mintova, J. P. Gilson, V. Valtchev, *Nanoscale* **2013**, *5*, 6693; b) C. S. Cundy, P. A. Cox, *Chem. Rev.* **2003**, *103*, 663.
- [12] a) M. Moliner, F. Rey, A. Corma, *Angew. Chem., Int. Ed.* **2013**, *52*, 13880; b) T. Ryu, N. H. Ahn, S. Seo, J. Cho, H. Kim, D. Jo, G. T. Park, P. S. Kim, C. H. Kim, E. L. Bruce, P. A. Wright, I. S. Nam, S. B. Hong, *Angew. Chem., Int. Ed.* **2017**, *56*, 3256; c) J. H. Lee, M. B. Park, J. K. Lee, H.-K. Min, M. K. Song, S. B. Hong, *J. Am. Chem. Soc.* **2010**, *132*, 12971.
- [13] a) H. Xu, J. Zhang, Q. M. Wu, W. Chen, C. Lei, Q. Y. Zhu, S. C. Han, J. H. Fei, A. M. Zheng, L. F. Zhu, X. J. Meng, S. Maurer, D. Dai, A. N. Parvulescu, U. Muller, F. S. Xiao, *ACS Appl. Mater. Interfaces* **2019**, *11*, 23112; b) N. Funase, T. Tanigawa, Y. Yamasaki, N. Tsumoji, M. Sadakane, T. Sano, *J. Mater. Chem. A* **2017**, *5*, 19245.
- [14] F. Delprato, L. Delmotte, J. L. Guth, L. Huve, *Zeolites* **1990**, *10*, 546.
- [15] T. Moteki, T. Okubo, *Chem. Mater.* **2013**, *25*, 2603.
- [16] A. Inayat, I. Knoke, E. Spiecker, W. Schwieger, *Angew. Chem., Int. Ed.* **2012**, *51*, 1962.
- [17] V. Valtchev, L. Tosheva, *Chem. Rev.* **2013**, *113*, 6734.
- [18] Y. J. Jiang, J. Huang, W. L. Dai, M. Hunger, *Solid State Nucl. Magn. Reson.* **2011**, *39*, 116.
- [19] a) S. C. Larsen, *J. Phys. Chem. C* **2007**, *111*, 18464; b) V. J. Margarit, M. R. Diaz-Rey, M. T. Navarro, C. Martinez, A. Corma, *Angew. Chem., Int. Ed.* **2018**, *57*, 3459.
- [20] A. I. Lupulescu, J. D. Rimer, *Science* **2014**, *344*, 729.
- [21] D. W. He, D. H. Yuan, Z. J. Song, Y. S. Tong, Y. Q. Wu, S. T. Xu, Y. P. Xu, Z. M. Liu, *Chem. Commun.* **2016**, *52*, 12765.
- [22] G. X. Niu, Y. Huang, X. Y. Chen, J. M. He, Y. Liu, A. He, *Appl. Catal., B* **1999**, *21*, 63.
- [23] J. M. Silva, M. F. Ribeiro, F. R. Ribeiro, E. Benazzi, N. S. Gnep, M. Guisnet, *Zeolites* **1996**, *16*, 275.
- [24] J. L. Agudelo, E. J. M. Hensen, S. A. Giraldo, L. J. Hoyos, *Fuel Process. Technol.* **2015**, *133*, 89.